Effect of Multiple-Pass Friction Stir Processing Overlapping on Microstructure and Mechanical Properties of As-Cast NiAl Bronze

D.R. NI, P. XUE, and Z.Y. MA

As-cast Cu-9Al-4.5Ni-4Fe NiAl bronze alloy (NAB) was subjected to multiple-pass friction stir processing (FSP) with a 50 pct overlap. After FSP, the coarse microstructure of the base metal (BM) was transformed to defect-free material with fine microstructure. While the torchlike patterns in the stir zone (SZ) and the uplifted grains in the transitional zones (TZs) between two passes were observed in the multiple-pass FSP region, no grain coarsening was found in the remnant zone of the previous SZ after subsequent FSP pass. The hardness value of the FSP materials was higher than that of the BM and was homogeneously distributed throughout the entire multiple-pass FSP region. The FSP materials showed greatly improved tensile properties compared to the BM, and the TZs showed similar tensile strength and ductility to the single-pass FSP materials. The BM broke in a mixture mode of brittle cleavage and microvoid coalescence fracture, whereas the FSP and TZ samples failed in the latter fracture mode. The results showed that the multiple-pass overlapping (MPO) FSP was feasible to modify the microstructure of large-sized plate of the NAB.

I. INTRODUCTION

THE NiAl bronze alloy (NAB) is extensively used for propulsion and seawater handling systems[1–6] due to the high strength, good fracture toughness, and excellent erosion-corrosion resistance.[1–4,7] The as-cast NAB is characterized by coarse Widmanstätten α phase, nickel-iron-aluminum κ phases, and island martensite β′ phase, and the transformation products and their precipitation sequence are complex.[8–13] Furthermore, cast defects such as the shrinkage porosity and pores is a common problem for the NAB castings due to the poor casting properties. This microstructure is disadvantageous to the mechanical and corrosion properties of components. For example, the ASTM B148 cast alloy is used to make the ship propellers; however, the yield strength (YS) of slowly cooled regions in large propeller blades is typically 25 pct lower than the tensile property requirements for the keel block for this alloy (241 MPa).[14] Therefore, in order to improve the service life of the cast NAB components, it is necessary to refine the coarse as-cast structure and eliminate the porosity defects.

In the past decade, a multifunctional metal working technique named friction stir processing (FSP) has been rapidly developed based on the basic principles of friction stir welding (FSW), which was invented at The Welding Institute (TWI, United Kingdom) in 1991.[15–17] This technique was first used by Mishra et al. to produce fine-grained aluminum alloys,[18,19] and then applied to modify the heterogeneous microstructure,[20] produce surface composites,[21,22] and synthesize composites and intermetallic compounds.[23,24] An important function of FSP is to provide localized modification and control of microstructure in the near-surface region of castings without changing the shape of components, with the aim to repair defects and to refine and homogenize the coarse microstructures. This provides a simple and promising way to solve the problem of the NAB, as mentioned previously.

Previous investigations showed that FSP could effectively refine the coarse microstructure of the NAB, heal the porosity defect, and homogenize the microstructure, thereby increasing the hardness, tensile properties, fatigue strength, and corrosion resistance.[14,25–27] Oh-ishi and co-workers[28–32] reported that the main characteristic of the stir zone (SZ) of the FSP NAB was inhomogeneous microstructures in various subregions, including Widmanstätten structure, equiaxed fine grain structure, and banded or lamellar structure. Similar results were also reported by Mahoney et al.[25] and Fuller et al.[33] More recently, our study further showed that the inhomogeneous microstructure was parameter dependent, and both the hardness and tensile properties of the as-cast NAB were greatly increased by FSP.[34] Furthermore, the FSP sample showed much lower corrosion rate in the static immersion corrosion condition in neutral salt solution and a tiny variation in electrochemical corrosion resistance.[35]

In practice, using FSP to modify the microstructure or heal the defects of a large-sized cast components means that multiple-pass overlapping (MPO) FSP with a certain level of overlap between the successive passes

D.R. NI, Assistant Professor, P. XUE, Postgraduate, and Z.Y. MA, Professor, are with the Shenyang National Laboratory for Materials Science, Institute of Metal Research, Chinese Academy of Sciences, Shenyang 110016, P.R. China. Contact e-mail: zyma@imr.ac.cn

should be applied. The MPO FSP mode is quite different from the single-pass mode, because the subsequent pass generates the heat-affected zone (HAZ) and thermomechanically affected zone in the SZ of the previous pass. In this case, it is important to understand the microstructure evolution during the MPO FSP and its influence on the mechanical properties.

The MPO FSP of the cast NAB was previously reported,[14,26,36] and the effect of raster patterns (linear and rectangular spiral raster patterns) on the mechanical properties of the FSP material was compared. However, details such as the microstructure and mechanical properties of the transitional zones (TZs) between two FSP passes were not discussed. In our previous studies, we reported that a single pass of FSP on the cast NAB could produce densified fine-grained material with good mechanical properties and corrosion resistance.[34,35] In this study, we conducted the MPO FSP of the cast NAB. The aim is to examine the microstructure evolution and mechanical properties of the microregions in the MPO FSP cast NAB.

II. EXPERIMENTAL

The 10-mm-thick commercial UNS C95800 NAB alloy sand-cast plates with a composition of 9.18Al-4.49Ni-4.06Fe-1.03Mn-bal Cu (in wt pct) were used in this study. The as-received NAB plates were machined into pieces with a dimension of $300 \times 70 \times 8$ mm^3. FSP was performed under a tool rotation rate of 1200 rpm and a traverse speed of 50 mm min^{-1} with a tool tilt angle of 3 deg. A nickel-based superalloy tool with a concave shoulder 24 mm in diameter and a threaded conical pin 8 mm in root diameter and 7 mm in length were used. Both the tool and the processed workpiece were subjected to blow over cooling during FSP. A linear raster pattern with three passes was adopted (Figure 1). After each FSP pass, the pin was moved 5 mm from the center of the former pass, which was determined based on the size of the cross section of the single-pass FSP (Figure 2(a)). The FSP plate was cooled to room temperature prior to the next FSP pass to eliminate the effect of accumulative heating. All the FSP passes were toward the same direction with the retreating side (RS) being overlapped.

The microstructure of the base metal (BM) and the FSP samples were examined using optical microscopy (OM) after etching with solution of 5 g FeCl$_3$ + 2 mL HCl + 95 mL C$_2$H$_5$OH. The hardness profiles were measured along the midheight of the SZ on the transverse cross section using a LECO-LM-247AT*

---

*LECO is a trademark of LECO Corporation, St. Joseph, MI.

---

micro-Vickers hardness tester with a load of 5 kg for 15 seconds. Three kinds of minitensile testing samples were prepared perpendicular to the FSP direction to measure the tensile properties of the FSP material. Dogbone-shaped tensile specimens with a gage dimension of
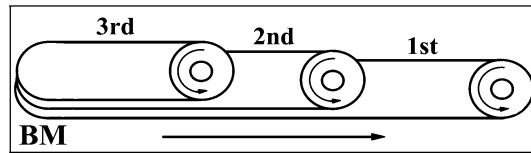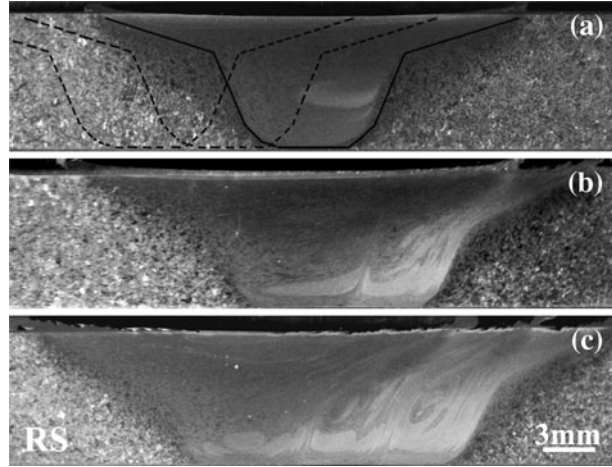

Fig. 1—Schematic diagram of MPO FSP.

Fig. 2—Optical cross-sectional macrograph of FSP NAB samples: (a) single-pass and raster pattern, (b) two-pass overlapping, (c) three-pass overlapping.

$5 \times 1.5 \times 0.85$ mm^3, $10 \times 1.5 \times 0.85$ mm^3, and $15 \times 1.5 \times 0.85$ mm^3 were machined, perpendicular to the FSP direction, with the gage center in the center of the single-pass FSP sample and the TZs, the two-pass overlapping FSP sample, and the three-pass overlapping FSP sample, respectively. Tensile specimens of the BM were also prepared with a gage dimension of $10 \times 1.5 \times 0.85$ mm^3 for comparison. Tensile tests were conducted at a strain rate of 1×10^{-3} s^{-1} at room temperature, using an Instron** 5848 tensile tester. The

---

**INSTRON is a trademark of Instron Corporation, Norwood, MA.

---

property data for each condition were obtained by averaging four test results. The fracture surfaces were examined on a scanning electron microscope (SEM, Quanta† 600).

---

†Quanta is a trademark of FEI Company, Hillsboro, OR.

III. RESULTS

A. Optical Microstructure

Figures 2(a) through (c) show the optical cross-sectional macrographs of the SZs of the single-pass, two-pass, and three-pass overlapping FSP samples, respectively. All the SZs showed the basinlike shape with a wide top region, and the width of the SZs
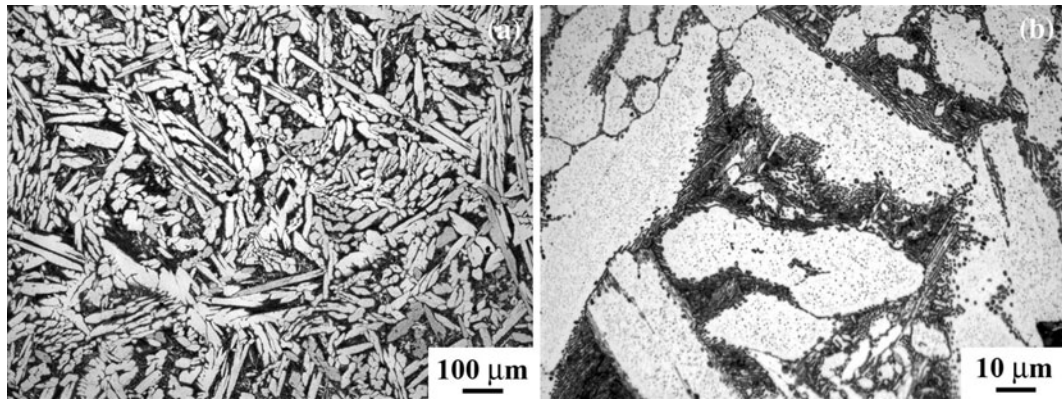
Fig. 3—Optical microstructure of as-cast NAB: (*a*) Widmanstätten morphology and porosities and (*b*) precipitates.

increased as the passes increased. The microstructure of the BM was composed of coarse Widmanstätten α phase, coarse martensite β' phase, and fine κ phase particles (Figure 3). Casting defects such as porosities were also found in the as-cast alloy due to the poor casting properties. Two kinds of phases could be identified in Figure 3. The light-etching phase was the α phase, which was about 150 μm in size. The dark-etching constituents were associated with the various β phase transformation products.

The dotted lines in Figure 2(a) marked the positions where the second and third passes would appear. The purpose of locating the unperformed FSP passes was to ensure that no unstirred areas remained after the MPO FSP. From Figure 2(a), the distance between two passes was determined to be 5 mm, which was adopted to perform the MPO FSP. In Figure 2(b), a white torchlike pattern was found in the remnant region of the first FSP, which showed the material flow pattern during FSP. The TZ between the two passes was nearly invisible at the upper part of the SZ, whereas it was discernible at the lower part. In Figure 2(c), two white torchlike patterns were found in the remnant regions of the first and second FSPs, respectively. Compared to the BM, the microstructures in the SZs were obviously refined and densified.

In the single-pass FSP sample (Figure 2(a)), an "onion ring" flow pattern was observed around the center, and the microstructure could be divided into four subregions from the surface to the bottom (Figure 4). Figure 5 shows the typical microstructure in the four regions at a higher magnification: fine Widmanstätten primary α phase in the surface layer (Figure 5(a)), banded primary α and β' phases in the subsurface layer (Figure 5(b)), equiaxed α and β' phases with a size of less than 10 μm in the center (Figure 5(c)), and streamlike α and β' phases at the bottom (Figure 5(d)). The center region possessed most of the SZ, in which few α phase and partial κ phases transformed into the β phase during FSP, and most of the α phase converted into equiaxed grains due to the dynamic recrystallization resulting from severe deformation.

Figures 6(a) through (f) show the microstructures of various regions in Figure 2(b). The remnant region of the first FSP showed apparent flow patterns, especially in the advancing side (AS) (Figure 6(a)), whereas the

counterpart of the second FSP was homogenous and no flow pattern was found (Figure 6(b)). The 2nd FSP showed the onion ring flow pattern (Figure 6(c)). The TZ between the two passes showed different macrostructures from the top to bottom, *i.e.*, slight flow pattern in the top (Figure 6(d)), the mixture of two flow patterns in the center part (Figure 6(e)), and two distinguishable patterns in the bottom (Figure 6(f)).

Figures 7(a) through (e) show the microstructures of various regions in Figure 2(c). The remnant regions of the first and second FSPs showed the torchlike flow pattern (Figures 7(a) and (b)), but the latter was greatly weakened. The third FSP also exhibited the onion ring pattern (Figure 7(c)). The microstructure in the TZ between the first and second passes (1 to 2 TZ) showed apparent flow patterns (Figure 7(d)), whereas the TZ between the second and third passes (2 to 3 TZ) was much more homogenous (Figure 7(e)). It was found at a high magnification that the α and β phases in various SZs of first, second, and third FSPs in the three-pass overlapping FSP samples showed similar sizes (Figure 8).

B. *Microhardness*

The hardness profiles of the single-pass FSP, two-pass overlapping FSP, and three-pass overlapping FSP samples are all shown in Figure 9. Three important observations can be made. First, the hardness value of the FSP samples was significantly higher than that of the BM. Second, the BM showed a fluctuated hardness value, whereas the FSP materials exhibited a relatively homogeneous hardness distribution. Third, the hardness value on the right hand of the three-pass overlapping sample is consistent with that of the two-pass overlapping and single-pass samples.

C. *Tensile Properties and Fractography*

The tensile properties of the as-cast NAB alloy and the FSP samples are shown in Table I. As can be seen, both the tensile strength and the ductility of the BM were greatly improved after a single-pass FSP. Along the transverse direction, the YS and ultimate tensile strength (UTS) of the single-pass FSP sample increased by 67 and 35 pct, respectively. Compared to the single-pass FSP,
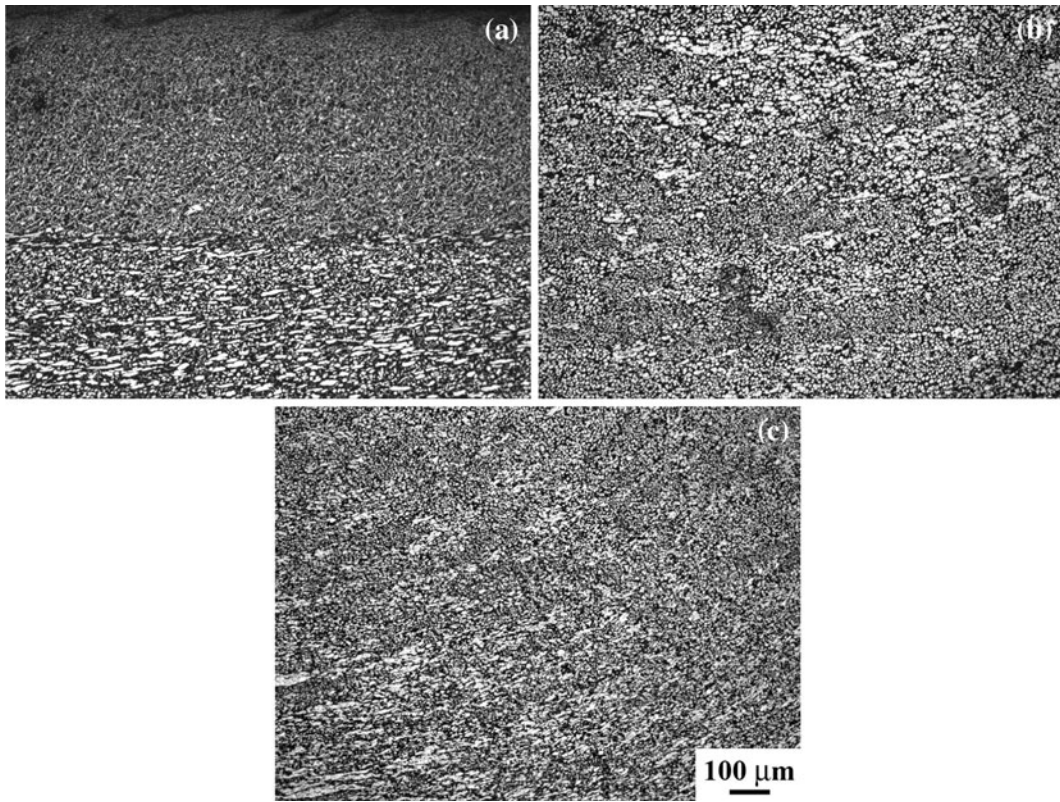
Fig. 4—Optical microstructures in SZ of single-pass FSP NAB: (*a*) surface and subsurface layer, (*b*) center, and (*c*) bottom.
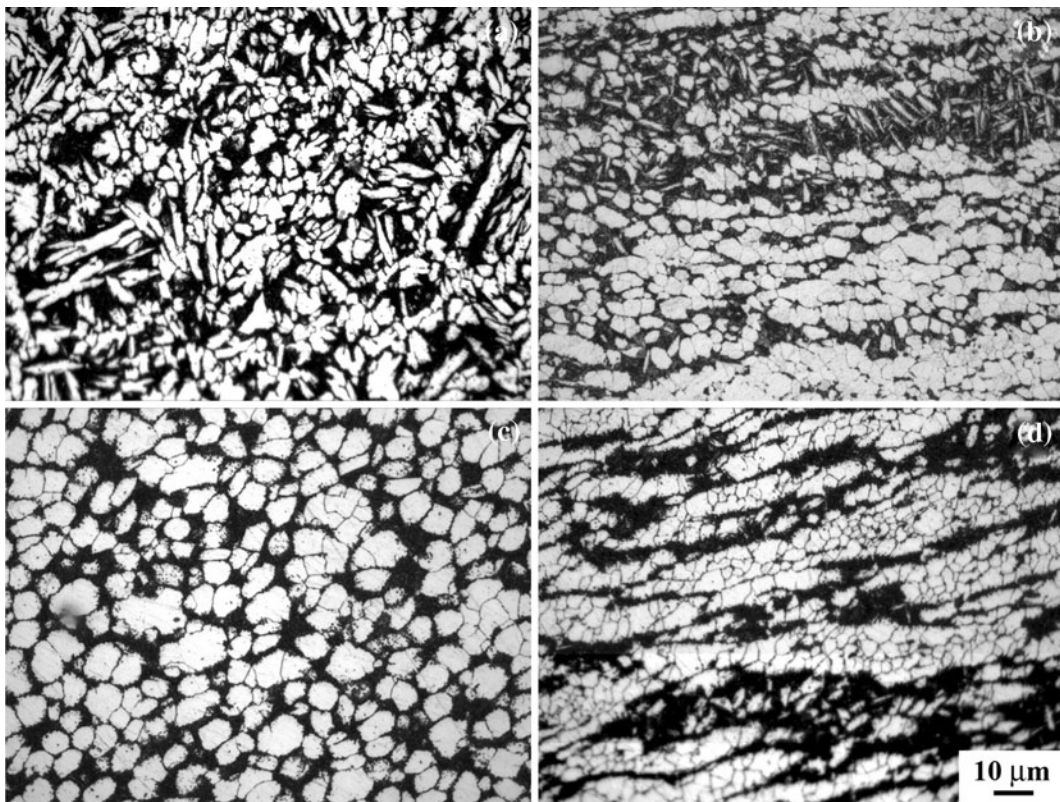

Fig. 5—Different microstructures in SZ of single-pass FSP NAB at high magnification: (*a*) surface layer, (*b*) subsurface layer, (*c*) center, and (*d*) bottom.
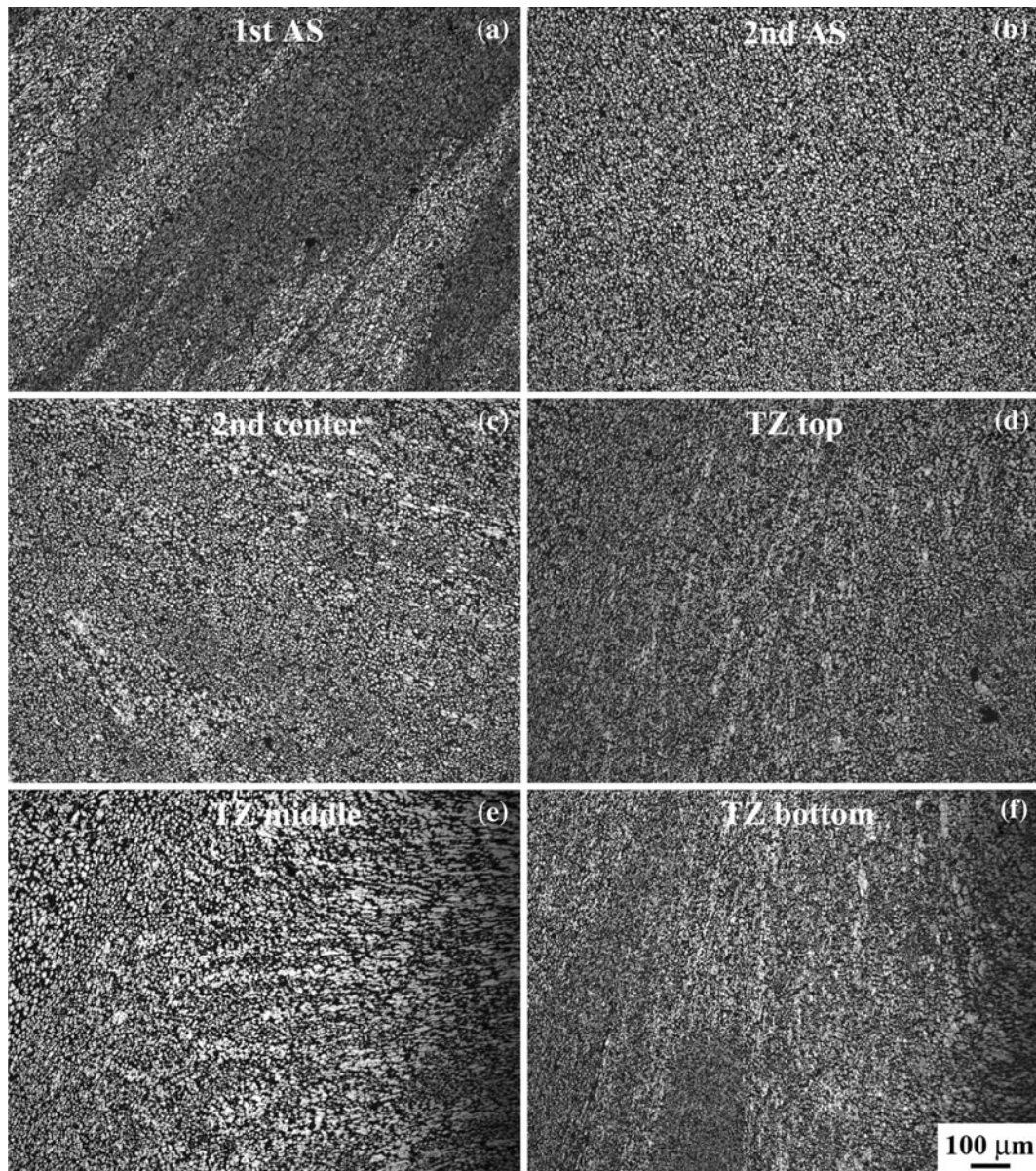
Fig. 6—Optical microstructure in SZ of two-pass overlapping FSP NAB: (*a*) first AS, (*b*) second AS, (*c*) second center, (*d*) TZ top, (*e*) TZ middle, and (*f*) TZ bottom.

both the two-pass and three-pass overlapping SZs showed the same level of YS and UTS, respectively. In the two-pass overlapping sample, the TZ showed similar YS and UTS compared to the entire SZ. In the three-pass overlapping sample, both the 1–2 TZ and 2–3 TZ showed similar YS, UTS, and elongation compared to the TZ in the two-pass overlapping sample. Although it is not appropriate to compare the ductility of various samples due to different gage lengths of the tensile specimens, the results revealed that the FSP improved the ductility of the BM and the MPO FSP did not decrease the elongation of the single-pass FSP samples.

For the MPO FSP samples, the fracture occurred randomly in the gage length and no preferential fracture at the special locations, such as the TZs between two successive FSP passes or the HAZ caused by subsequent FSP pass, was observed, indicating a relatively uniform property distribution throughout the entire FSP region produced by the MPO.

The fracture surface of the BM, single-pass FSP, TZ of two-pass overlapping FSP, and 1–2 and 2–3 TZs of three-pass overlapping FSP samples are shown in Figures 10(a) through (e), respectively. The fracture surface of the BM was rough and was composed of large tear ridges and small dimples (Figure 10(a)). Meanwhile, some cracks were visible on the surface. By comparison, the fracture surface of the single-pass FSP sample was relatively even and mainly composed of small dimples without cracks (Figure 10(b)). The fracture surfaces of all the TZ samples were even and
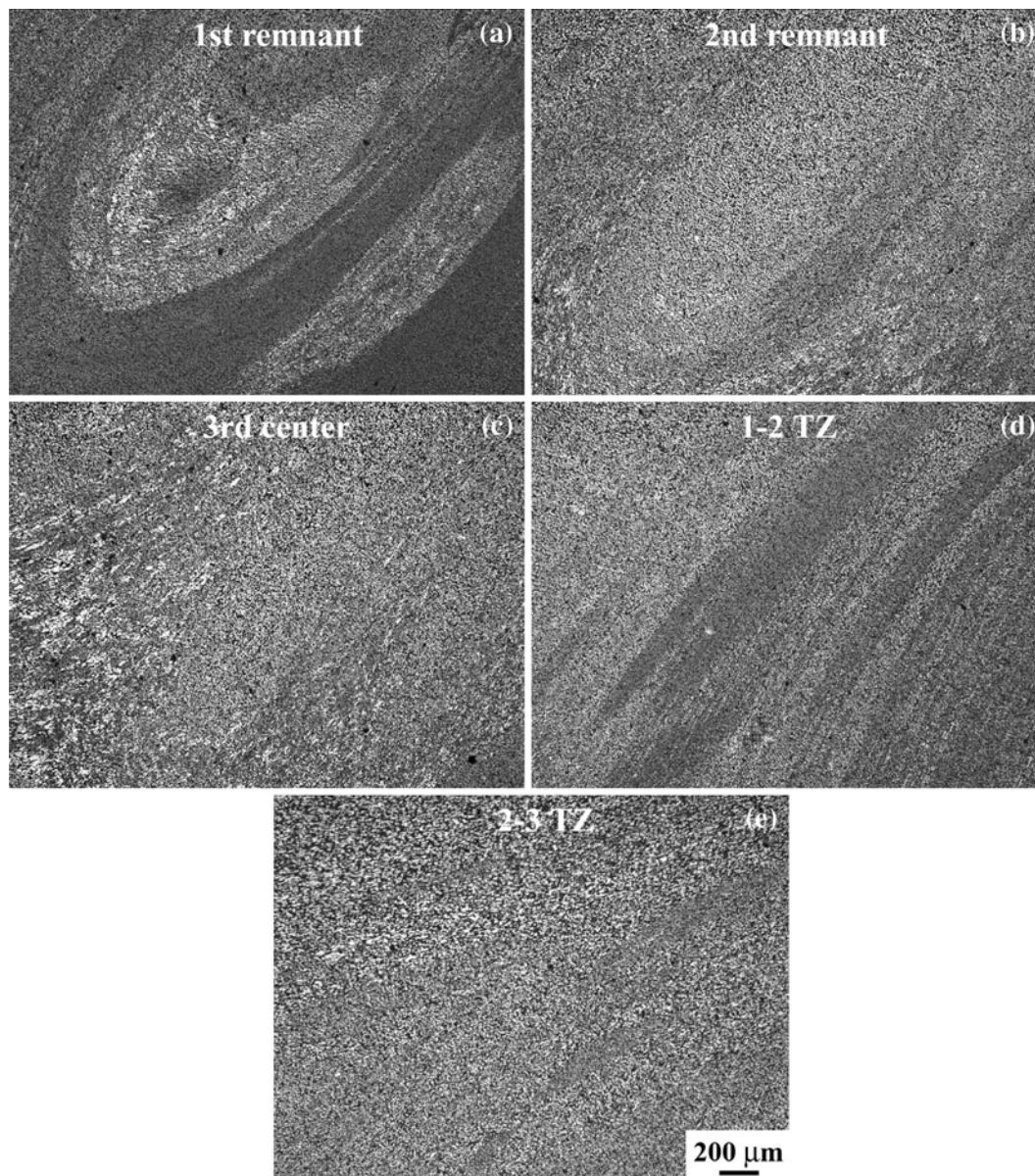
Fig. 7—Optical microstructure in SZ of three-pass overlapping FSP NAB: (*a*) first remnant region, (*b*) second remnant region, (*c*) third center, (*d*) 1–2 TZ, and (*e*) 2–3 TZ.

similar, and the dimples were deeper and distributed more homogeneously compared to that of the single-pass FSP sample (Figures 10(c) through (e)).

IV. DISCUSSION

A. *Microstructural Characteristics*

The typical microstructure of the as-cast NAB was composed of coarse Widmanstätten α phase, nickel-iron-aluminum κ phases, and island martensite β' phase; furthermore, casting defects of shrinkage porosity were also found (Figure 3). After FSP, the coarse microstructure of the BM was greatly refined and densified (Figure 4), and it has been discussed in detail in our previous report.[34]

For the two-pass overlapping FSP (Figure 2(b)), the flow patterns were macroscopically visible in the AS of the first FSP (Figure 6(a)), whereas no onion ring patterns were found in the second AS (Figure 6(b)). The more homogenous microstructure in the second AS was attributed to the double FSP effect, because this region was processed during both the first and second FSPs. This means that the multiple-pass FSP was beneficial to the microstructure homogenization. Similarly, it was reported that the two-pass FSP with a 100 pct overlap produced more homogeneous microstructure in AZ80 magnesium alloy casting than single-pass FSP.[37] The microstructure in the center of the second FSP was similar to that in the single-pass FSP (Figure 6(c)). The TZ between the two passes showed different macrostructures from the top to the bottom
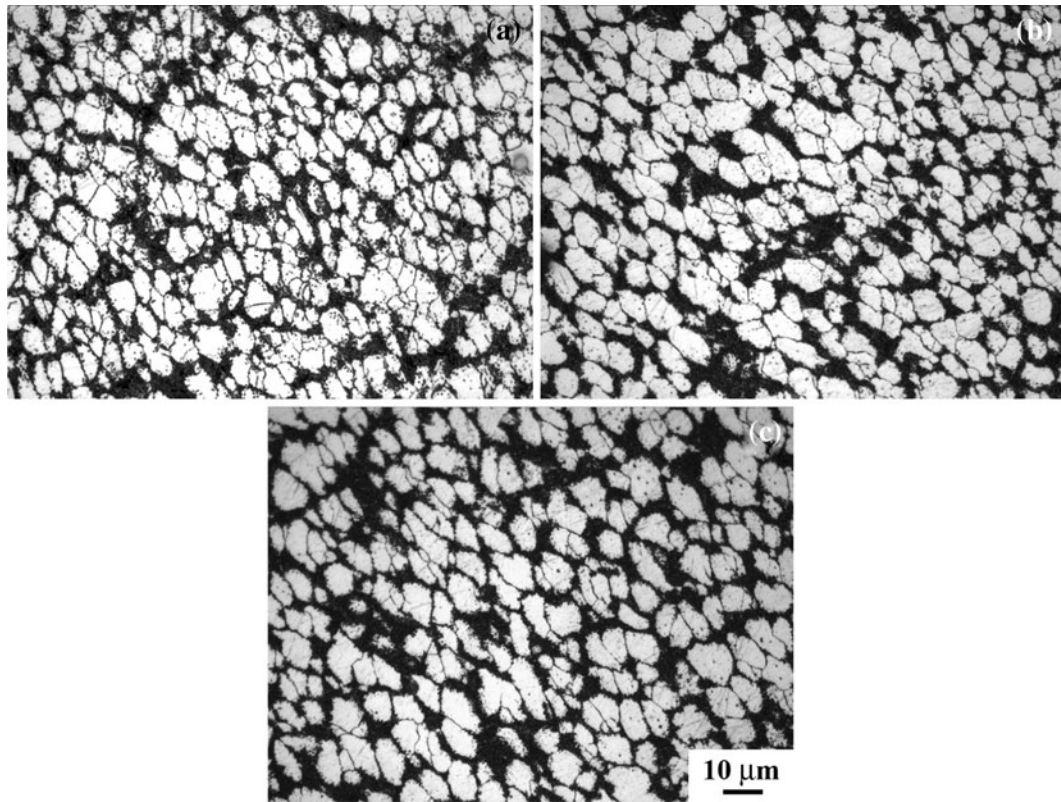
Fig. 8—Optical microstructure of SZ in three-pass overlapping FSP NAB at high magnification: (a) remnant region of first SZ, (b) remnant region of second SZ, and (c) center of third SZ.
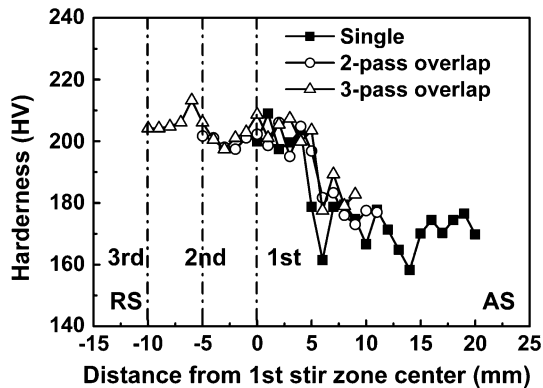

Fig. 9—Microhardness profiles of cross section of FSP NAB samples.

(Figures 6(d) through (f)). This was due to the different flow patterns of materials from the top to the bottom. The torchlike flow pattern and uplifted grains in the TZ were due to the switching between the advancing and RSs of each pass.

For the three-pass overlapping FSP (Figure 2(c)), the torchlike flow patterns in the remnant regions of the first and second FSPs were obvious (Figures 7(a) and (b)), but the latter was greatly weakened and this was due to the effect of multiple-pass FSP. The right and left sides of the second FSP are essentially coincident with the left side of the first FSP and the right side of the third FSP, respectively. The center of the third FSP was similar to that of the single-pass FSP (Figure 7(c)). Compared to the 1–2 TZ (Figure 7(d)), the 2–3 TZ (Figure 7(e)) exhibited the greatly alleviated flow patterns and the

Table I. Tensile Properties of As-Cast and FSP NAB Samples

FSP Pass	Sample	YS (MPa)	UTS (MPa)	EL (Pct)
—	as-cast	254 ± 4	585 ± 57	21.0 ± 6.6
Single	SZ	423 ± 32	789 ± 18	26.0 ± 1.3
Two-pass	TZ	437 ± 15	793 ± 12	27.7 ± 1.1
	overlapping SZ	422 ± 16	788 ± 12	26.7 ± 1.4
Three-pass	1–2 TZ	466 ± 14	793 ± 15	26.5 ± 2.5
	2–3 TZ	449 ± 11	807 ± 4	28.4 ± 2.4
	overlapping SZ	452 ± 29	783 ± 25	26.3 ± 1.2

Gage dimension: $10 \times 1.5 \times 0.85$ mm^3 for as-cast, $5 \times 1.5 \times 0.85$ mm^3 for single SZ and TZ, $10 \times 1.5 \times 0.85$ mm^3 for two-pass overlapping SZ, and $15 \times 1.5 \times 0.85$ mm for three-pass overlapping SZ.
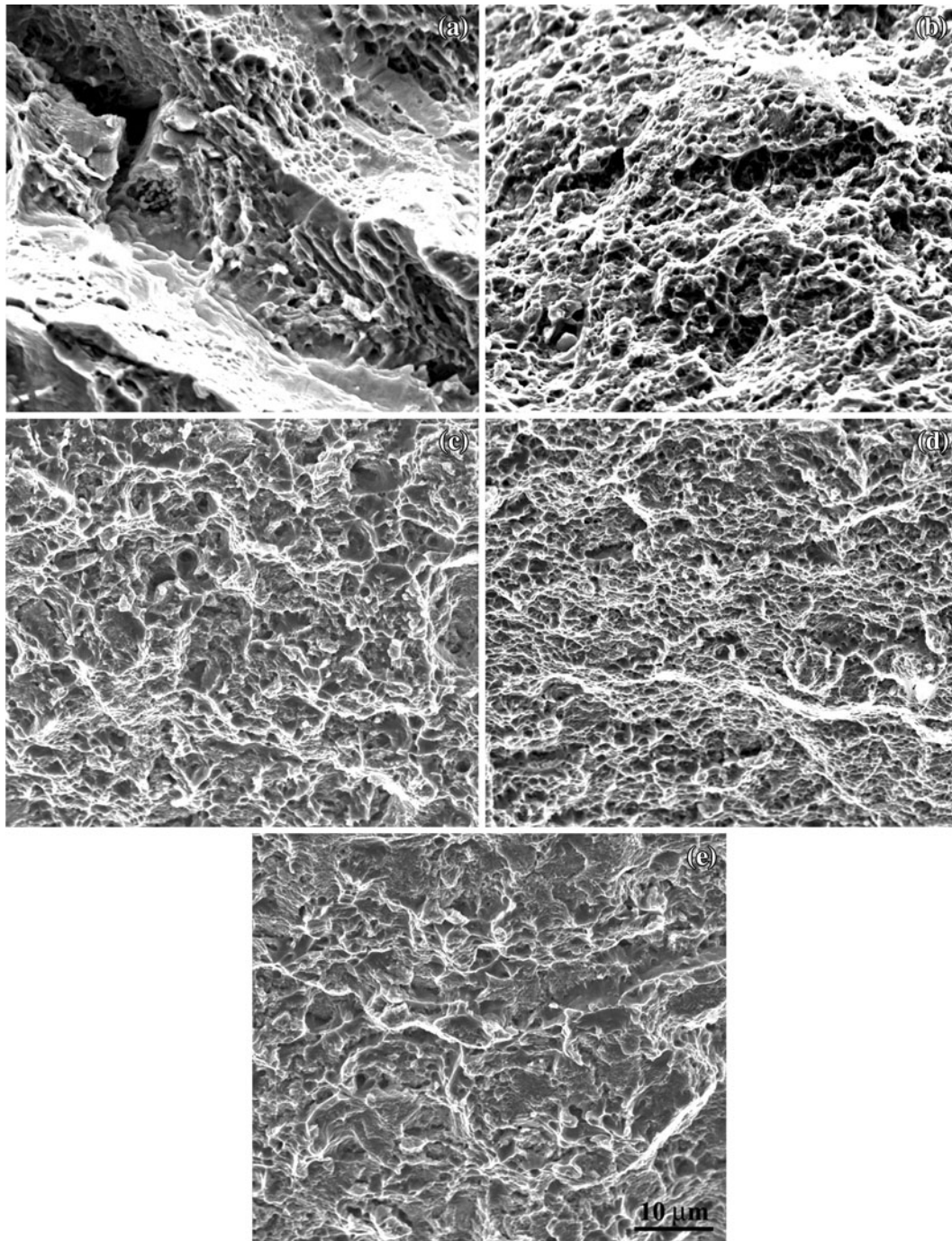
Fig. 10—SEM fractographs of NAB: (*a*) as-cast, (*b*) single-pass FSP, (*c*) TZ of two-pass overlapping FSP, (*d*) 1–2 TZ, and (*e*) 2–3 TZ of three-pass overlapping FSP.

microstructure was more homogenous because of more FSP passes. The result showed that as the number of the FSP pass increased over a certain level, the TZs in the MPO FSP material became fundamentally homogeneous. The α and β phases in various SZs of the three-pass overlapping FSP sample showed little difference both in the morphology and the sizes (Figure 8). This indicates that the heat generated by the subsequent passes did not coarsen the fine grains produced by the former FSP.

Palko *et al.*[14] first reported the MPO FSP of the cast NAB, in which the processed area was created by a series of FSP passes, which rastered across the sample in the same direction with a stepover of 1 pin diameter. Rastering of the FSP passes aided in reducing the nonuniformity within the processed zone by eliminating the previous RS of a FSP pass with the AS of the adjacent pass. However, the microstructure of the MPO FSP NAB was not fully described and the tensile strength was not reported, so we were unable to evaluate

this MPO mode. Fuller et al.[26] and Mahoney et al.[36] investigated a series of raster approaches for the MPO FSP of the cast NAB. Their results showed that, for linear patterns, if the tool rotation direction was not changed following the completion of each pass, the AS and RS microstructure zones were produced, and this resulted in an inhomogeneous processed zone. This kind of structure was consistent with our result. For a rectangular spiral out raster pattern with the AS on the interior of the pattern, the microstructure was more homogeneous, but the AS material was created during each pass resulting in a distinct vertical flow of material between passes.[26,36] They considered that this AS or interpass microstructure was softer than the adjacent processed material. However, for this rectangular pattern, changing the tool travel direction moved the AS microstructure to the raster boundary, thus a SZ with homogeneous and fine grain microstructure was generated without the banded interpass microstructure, and they considered this kind of microstructure beneficial to the ductility.

B. Microhardness

The horizontal hardness profiles along the midheight of the SZ center of the single-pass, two-pass overlapping, and three-pass overlapping FSP samples indicated that FSP improved the hardness of the as-cast NAB (Figure 9). The increase of the hardness should be attributed to the microstructure refinement and the elimination of the casting defects in the BM. On the one hand, according to the Hall–Patch relationship, the microstructure refinement of the coarse BM could provide higher hardness. On the other hand, the casting porosities in the BM were closed during FSP, and this was certainly beneficial to the increase and homogenization of hardness. The hardness of the overlapping FSP samples was in agreement with that of the single-pass FSP sample. This result showed that no weakened region appeared in the MPO FSP materials, and this was consistent with the results of Palko et al.,[14] in which the microhardness across the rastered microstructure showed a uniform distribution within the processed zone. Although nearly 50 pct of the SZ area was overlapped, the hardness value of the repeated FSP region did not increase. This was in good agreement with our previous study, in which the in-situ two-pass FSP sample did not exhibit higher hardness value than the single-pass one.[34] The hardness values of the present MPO FSP samples are consistent with the previous reports, in which the hardness values of about 190 to 220 Hv and 190 to 215 Hv were recorded for 9- and 20-mm-thick FSP NAB, respectively.[14] This means that the MPO mode adopted here did not decrease the hardness value of the FSP materials.

C. Tensile Properties and Fractography

Both the single-pass and the MPO FSP samples exhibited significantly improved tensile strength and ductility compared to the as-cast NAB (Table I). The improvement in the tensile properties of the FSP NAB

was ascribed to the refinement of the coarse microstructure and the elimination of the casting defects, as discussed for the increase of the hardness. The strength of the two-pass and three-pass overlapping samples was at the same level as that of the single-pass FSP sample, and this indicates that increasing the number of overlapping FSP passes hardly affects the tensile properties of the overlapping NAB. Both the 1–2 TZ and 2–3 TZ in the three-pass overlapping sample showed similar strength and elongation to the TZ in the two-pass overlapping sample, indicating that the tensile properties of the TZ were stable and were not visibly affected by the subsequent passes.

Fuller et al.[26] reported that the YS and UTS of the MPO FSP NAB were 504 to 522 MPa and 765 to 805 MPa in a linear raster pattern and 460 to 507 MPa and 743 to 761 MPa in a rectangular raster pattern, respectively. The linear pattern showed a higher tensile strength and a lower ductility compared to the rectangular pattern, and the lower ductility was attributed to the inhomogeneous microstructure. Meanwhile, changing the raster pattern from linear to rectangular spiral slightly lowered the overall fatigue resistance, but it did not produce any significant change in fatigue data scatter. These results revealed that, although the linear raster pattern generated the torchlike structure in the SZ, it may provide better mechanical properties for the MPO FSP materials. Compared to their results, the YS values in the present study were lower, whereas the UTS values were similar.

The tensile strengths of the present MPO FSP NAB were better than those of the single-pass FSP NAB reported by Palko et al.[14] in which the YS and UTS were 400 to 420 MPa and 689 to 724 MPa, respectively, and those reported by Mahoney et al.[25] in which the YS and UTS are 433 and 741 MPa, respectively. Meanwhile, the tensile strengths were lower than our previously reported results for the single-pass FSP NAB,[34] and this may be due to the BMs, which came from different batches. Because the tensile specimens with different dimensions were used in this study, it is impossible to compare the present elongation values with the previous ones (14 to 16 pct and 23 pct in References 14 and 25, respectively). However, the present results indicated that the MPO FSP materials had a proper ductility.

Santella et al.[38] reported the MPO FSP on as-cast A356 and A319 alloys with five to six passes overlapping at intervals of about 4 mm. After FSP, the microstructures were refined and homogenized, and the visible porosity and dendritic microstructures were eliminated. The transverse samples covering the entire FSP region produced by the MPO FSP showed better UTS, ductility, and fatigue life compared to the BM, showing that the MPO FSP is useful for engineering applications of these alloys. However, they did not provide an insight into the correlation between the intrinsic tensile properties and the localized microstructure. Ma et al.[39] further investigated the effect of MPO, five pass with 50 pct overlapping, on the microstructure and tensile properties of cast A356 alloy. The overlapping FSP did not exert a significant effect on the size and distribution

of the Si particles. The strength and ductility of the TZs between two FSP passes were slightly lower than those of the SZs, and the previously processed zones showed lower strength compared to the subsequently processed zones due to overaging from the FSP thermal cycles. However, after T6 heat treatment, the tensile properties of the five-pass FSP A356 samples were similar across various passes and comparable to those of the single-pass FSP sample. Their results showed that the thermomechanical history of the subsequent FSP passes did generate adverse effects on the MPO FSP materials. However, this phenomenon was not found in the present study, and this should be attributed to the fact that the NAB was less sensitive to heat treatment compared to the A356 alloy.

The fracture surface of the BM (Figure 10(a)) was rough and covered with large tear ridges, small dimples, and cracks, indicating that the sample broke in the manner of brittle cleavage and ductile microvoid coalescence fracture mode. This is attributed to the presence of the coarse hard and brittle martensite β' phase, the segregated κ-phase particles, and the casting porosities, which resulted in easy initiation and propagation of cracks. Due to the effect of the microstructure refinement, homogenization, and densification, the single-pass FSP sample exhibited a relatively even fracture surface, which was mainly composed of small dimples without tear ridges and cracks, and it failed in the microvoid coalescence fracture mode (Figure 10(b)). The present result was in agreement with that of Fuller et al.[33] This fracture surface further indicated that the FSP samples showed better tensile strength and elongation than the BM.

The effect of the grain refinement by FSP on the fracture behavior was also reported by Feng and Ma.[40] Their results showed that the as-cast AZ91D magnesium alloy exhibited a brittle fracture mode, and the coarse eutectic β-$Mg_{17}Al_{12}$ network at the grain boundaries was prone to crack or debond from the magnesium matrix, whereas the FSP sample exhibited a typical ductile dimple fracture, because FSP resulted in significant breakup and dissolution of the coarse eutectic β phase and remarkable grain refinement.

Compared to that of the single-pass FSP sample, the TZ samples also broke in the microvoid coalescence fracture mode, and the dimples on the fracture surfaces were deeper and distributed more homogeneously (Figures 10(c) through (e)). This was due to the fact that the TZs received multiple passes of FSP, and their microstructure was more homogeneous. All the TZs showed similar fracture surfaces, and this indicates that the MPO FSP did not affect the fracture behavior of the overlapping samples, and this can be further proved by the randomly distributed fracture positions.

V. CONCLUSIONS

1. MPO FSP greatly refined the microstructure of the as-cast NAB and generated a defect-free SZ. During FSP, the switching between AS and RS of each pass generated the torchlike patterns in the SZ and the uplifted grains in the TZs.
2. The heat generated by the following passes did not coarsen the fine grains of the former FSP. For the three-pass overlapping NAB, the α and β phases in the three SZs showed little difference both in the morphology and the size.
3. The FSP materials showed significantly higher hardness value and more homogeneous hardness distribution than the BM. The hardness value of the MPO FSP materials was similar to that of the single-pass FSP without weakened region.
4. The MPO FSP materials showed greatly improved tensile properties compared to the BM. The YS, UTS, and elongation were about 422 MPa, 788 MPa, and 26.7 pct, respectively, for the two-pass FSP sample, and about 452 MPa, 783 MPa, and 26.3 pct, respectively, for the three-pass FSP sample. The TZs showed similar strengths and elongation to the single-pass FSP material.
5. The FSP sample showed an even fracture surface composed of small dimples, which failed in a microvoid coalescence fracture mode. Compared to the FSP sample, the TZ samples showed similar fracture surfaces with the dimples being deeper and distributed more homogeneously.

REFERENCES

1. E.A. Culpan and G. Rose: *Br. Corros. J.*, 1979, vol. 14, pp. 160–66.
2. R.J. Ferrara and T.E. Caton: *Mater. Perform.*, 1982, vol. 21, pp. 30–34.
3. G.W. Lorimer, F. Hasan, J. Iqbal, and N. Ridley: *Br. Corros. J.*, 1986, vol. 21, pp. 244–48.
4. C.H. Tang, F.T. Cheng, and H.C. Man: *Mater. Sci. Eng. A*, 2004, vol. 373, pp. 195–203.
5. G. Kear, B.D. Barker, K. Stokes, and F.C. Walsh: *J. Appl. Electrochem.*, 2004, vol. 34, pp. 1235–40.
6. G. Kear, B.D. Barker, K. Stokes, and F.C. Walsh: *J. Appl. Electrochem.*, 2004, vol. 34, pp. 1241–48.
7. A. Al-Hashem and W. Riad: *Mater. Charact.*, 2002, vol. 48, pp. 37–41.
8. E.A. Culpan and G. Rose: *J. Mater. Sci.*, 1978, vol. 13, pp. 1647–57.
9. M. Sahoo: *Trans. AFS*, 1982, vol. 90, pp. 913–26.
10. A. Jahanafrooz, F. Hasan, G.W. Lorimer, and N. Ridley: *Metall. Trans. A*, 1983, vol. 14A, pp. 1951–56.
11. E.A. Feest and I.A. Cook: *Met. Technol.*, 1983, vol. 10, pp. 121–24.
12. F. Hasan, J. Iqbal, and N. Ridley: *Mater. Sci. Technol.*, 1985, vol. 1, pp. 312–15.
13. F. Hasan, A. Jahanafrooz, G.W. Lorimer, and N. Ridley: *Metall. Trans. A*, 1982, vol. 13A, pp. 1337–45.
14. W.A. Palko, R.S. Fielder, and P.F. Young: *Mater. Sci. Forum*, 2003, vols. 426–432, pp. 2909–14.

15. R.S. Mishra and Z.Y. Ma: *Mater. Sci. Eng. R*, 2005, vol. 50, pp. 1–78.
16. R. Nandan, T. DebRoy, and H.K.D.H. Bhadeshia: *Progr. Mater. Sci.*, 2008, vol. 53, pp. 980–1023.
17. P.L. Threadgill, A.J. Leonard, H.R. Shercliff, and P.J. Withers: *Int. Mater. R.*, 2009, vol. 54, pp. 49–93.
18. R.S. Mishra, M.W. Mahoney, S.X. McFadden, N.A. Mara, and A.K. Mukherjee: *Scripta Mater.*, 2000, vol. 42, pp. 163–68.
19. R.S. Mishra and M.W. Mahoney: *ICSAM-2000*, 2001, vols. 357–359, pp. 507–12.
20. P.B. Berbon, W.H. Bingel, R.S. Mishra, C.C. Bampton, and M.W. Mahoney: *Scripta Mater.*, 2001, vol. 44, pp. 61–66.
21. R.S. Mishra, Z.Y. Ma, and I. Charit: *Mater. Sci. Eng. A*, 2002, vol. 341, pp. 307–10.
22. A.S. Zarghani, S.F.K. Bozorg, and A.Z. Hanzaki: *Mater. Sci. Eng. A*, 2009, vol. 500, pp. 84–91.
23. C.J. Hsu, C.Y. Chang, P.W. Kao, N.J. Ho, and C.P. Chang: *Acta Mater.*, 2006, vol. 54, pp. 5241–49.
24. C.H. Chuang, J.C. Huang, and P.J. Hsieh: *Scripta Mater.*, 2005, vol. 53, pp. 1455–60.
25. M.W. Mahoney, W.H. Bingel, S.R. Sharma, and R.S. Mishra: *Mater. Sci. Forum,* 2003, vols. 426–432, pp. 2843–48.
26. C.B. Fuller, M.W. Mahoney, W.H. Bingel, M. Calabrese, and B. London: *Mater. Sci. Forum,* 2007, vols. 539–543, pp. 3751–56.
27. P.S. Prevey, D.J. Hornbach, and D.N. Jayaraman: *Mater. Sci. Forum,* 2007, vols. 539–543, pp. 3807–13.
28. K. Oh-ishi and T.R. McNelley: *Metall. Mater. Trans. A*, 2004, vol. 35A, pp. 2951–61.
29. K. Oh-ishi, A.M. Cuevas, D.L. Swisher, and T.R. McNelley: *Mater. Sci. Forum,* 2003, vols. 426–432, pp. 2885–90.
30. K. Oh-ishi and T.R. McNelley: *Metall. Mater. Trans. A*, 2005, vol. 36A, pp. 1575–85.
31. K. Oh-ishi, A.P. Zhilyaev, and T.R. McNelley: *Metall. Mater. Trans. A*, 2006, vol. 37A, pp. 2239–51.
32. T.R. McNelley, K. Oh-ishi, and A.P. Zhilyaev: *Mater. Sci. Forum,* 2007, vols. 539–543, pp. 3745–50.
33. M.D. Fuller, S. Swaminathan, A.P. Zhilyaev, and T.R. McNelley: *Mater. Sci. Eng. A*, 2007, vol. 463, pp. 128–37.
34. D.R. Ni, P. Xue, D. Wang, B.L. Xiao, and Z.Y. Ma: *Mater. Sci. Eng. A*, 2009, vol. 524, pp. 118–28.
35. D.R. Ni, B.L. Xiao, Z.Y. Ma, Y.X. Qiao, and Y.G. Zheng: *Corros. Sci.*, 2010, vol. 52, pp. 1610–17.
36. M.W. Mahoney, C. Fuller, W.H. Bingel, and M. Calabrese: *Mater. Sci. Forum,* 2007, vols. 539–543, pp. 3721–26.
37. A.H. Feng, B.L. Xiao, and Z.Y. Ma: *Metall. Mater. Trans. A*, 2009, vol. 40A, pp. 2447–56.
38. M.L. Santella, T. Engstrom, D. Storjohann, and T.Y. Pan: *Scripta Mater.*, 2005, vol. 53, pp. 201–06.
39. Z.Y. Ma, S.R. Sharma, and R.S. Mishra: *Scripta Mater.*, 2006, vol. 54, pp. 1623–26.
40. A.H. Feng and Z.Y. Ma: *Scripta Mater.*, 2007, vol. 56, pp. 397–400.